NUCL SCI TECH (2020) 31:37
https://doi.org/10.1007/s41365-020-0745-5

Advanced algorithms for retrieving pileup peaks of digital alpha spectroscopy using antlions and particle swarm optimizations

Mohamed S. El_Tokhy[1]

Received: 6 November 2019 / Revised: 5 February 2020 / Accepted: 5 February 2020 / Published online: 18 March 2020

Abstract Optimization algorithms are applied to resolve the second-order pileup (SOP) issue from high counting rates occurring in digital alpha spectroscopy. These are antlion optimizer (ALO) and particle swarm optimization (PSO) algorithms. Both optimization algorithms are coupled to one of the three proposed peak finder algorithms. Three custom time-domain algorithms are proposed for retrieving SOP peaks, namely peak seek, slope tangent, and fast array algorithms. In addition, an average combinational algorithm is applied. The time occurrence of the retrieved peaks is tested for an elimination of illusive pulses. Conventional methods are inaccurate and time-consuming. ALO and PSO optimizations are used for the localization of retrieved peaks. Optimum cost values that achieve the best fitness values are demonstrated. Thus, the optimum positions of the detected peak heights are achieved. Evaluation metrics of the optimized algorithms and their influences on the retrieved peaks parameters are established. Comparisons among such algorithms are investigated, and the algorithms are inspected in terms of their computational time and average error. The peak seek algorithm achieves the lowest average computational error for pulse parameters (amplitude and position). However, the fast array algorithm introduces the largest average error for pulse parameters. In addition, the peak seek algorithm coupled with an ALO or PSO algorithm is observed to realize a better performance in terms of the optimum cost and computational time. By contrast, the performance of the peak seek recovery algorithm is improved using the PSO. Furthermore, the computational time of the peak optimization using the PSO is much better than that of the ALO algorithm. As a final conclusion, the accuracy of the peaks detected by the PSO surpasses that for the peaks detected by the ALO. The implemented peak retrieval algorithms are validated through a comparison with experimental results from previous studies. The proposed algorithms achieve a notable precision for compensation of the SOP peaks within the alpha ray spectroscopy at a high counting rate.

Keywords Alpha spectrometry instrument · Second-order pileup · Signal processing · Optimization algorithms

✉ Mohamed S. El_Tokhy
engtokhy@gmail.com

[1] Engineering Department, NRC, Atomic Energy Authority, P. No. 13759, Inshas, Egypt

1 Introduction

Alpha particle spectroscopy has a significant importance in nuclear and experimental sciences [1, 2]. An alpha spectrometry instrument is utilized in recognition of alpha-emitting radionuclides [3]. High-resolution alpha spectroscopy helps achieve an accurate estimation of the source activity [4]. The performance of α-spectroscopy is improved using semiconductor detectors [1, 4]. The accuracy of α-spectroscopy is influenced by radiation sensors used in countless nuclear applications [5] such as nuclear security and safeguards [6]. One of these technologies is a scintillator [5], which allows recognition of the energy of the alpha sources [7] under high counting rate applications owing to its smallest pulse width. However, a second-order pileup (SOP) is a primary issue within alpha spectroscopy systems, especially at higher rates.

A higher probability of an SOP peak is achieved at higher counting alpha radiation rates for continuous or pulsed emissions [8]. An SOP is the pulse overlapping between three pulses [9], and is a general issue in alpha spectroscopy measurements, particularly at higher counting rates [10]. In other words, the SOP peak in α-spectroscopy represents an unavoidable distortion source [11]. The compound peaks are interpreted as a fictitious event. This peak is assigned to the error energy of an analogue-to-digital-converter (ADC) [11]. This error leads to distortions in the alpha spectra, image destruction in digital imaging structures [10], counting losses [12], attributes of the created pulse width, uncertainty [13], and dead-time in a data acquisition system (DAS) [8].

An SOP is a fundamental error source for distortion within alpha spectroscopy [14], and indicates the capturing of correct information from real signals [15]. An alpha pulse pileup has a serious influence on alpha spectroscopy techniques [15]. Overcoming the SOP issue saves 80% of the information along with a dead-time correction [15]. In addition, retrieval of an electronic SOP improves the detector throughput. SOP recovery techniques enhance the energy resolution and spectral accuracy [15]. In addition, the handling of an alpha SOP avoids the detector dead-time issue [15]. The retrieval and correction of an alpha SOP allow spectrometry to be applied at higher counting rates.

The compensation of a pulse pileup has been addressed by numerous researchers [16]. The research progress regarding the correction of a pileup in spectrometry applications is shown in Table 1. In [17], the author handles the pileup issue using a trapezoidal filter algorithm. This algorithm has the strength to tackle both the energy resolution and a ballistic deficit. Thus, it can be employed in nuclear applications worldwide [18]. The accuracy of such an algorithm is affected by the optimal selection of trapezoidal parameters [18]. Otherwise, the energy resolution of the deduced spectrum will deteriorate. In [14], the authors corrected an electronic pulse pileup using a true pulse shape algorithm. Information regarding the true pulse shape is necessary [14]. However, this algorithm is limited to a counting rate of 68 Kc/s because varied gain stability leads to unfavorable effects. In [19], the author aimed to correct a spectral distortion, and utilized a general function for overcoming a pileup. However, this method is limited to a lower energy background [19]. In [20], the authors applied a finite-length deconvolution filter for tackling the challenge of a pileup. In addition, their algorithm is applied in real time using a floating-point processor, i.e., a TMS320C6711. However, their accuracy is limited to 93%. In [21], two important algorithms are presented, namely pulse clipping and a modified phase-only correlation. These algorithms are implemented in the frequency domain, and can resolve adjacent peaks. They also show a much higher complexity, and thus a certain amount of computational cost will be involved.

The authors in [22] intended to overcome a pileup through the handling of higher counting rates in a spectrometry system. In addition, they presented a bimodal state-space method for realizing a quantitative analysis of higher particles rates [22]. A Kalman bimodal smoother is affected by the intrinsic statistical characteristics of the radiation signals, and is applied to obtain the optimal energy resolution and count rate under variant operating conditions [22, 23]. In [24], the authors applied a double-peak profile search algorithm for resolving overlapping pulses. Their method depends on an extraction of the features from the data using the relevant subspace (RS). These features are divided into several classification groups. A support vector machine is then functionalized for the training purposes of such features, and is intended as a classifier for classification of the combined set features. Although this algorithm is time-consuming, it lacks the need for high-speed spectrometry. Otherwise, the algorithm is supported through higher processing hardware.

Errors were previously not found in the measured spectra. Currently, they are accounted for through digital pulse acquisition systems [25]. Consequently, exceptional handling is a way to overcome this issue. It is crucial to account for SOP peaks in the recorded spectrum. A reduction in the instantaneous dose rate leads to a minimization of the SOP pulse [26]. Filtrations are applied as powerful techniques for overcoming and separating SOP pulses from each other [27]. A wide range of digital electronics within nuclear spectroscopy are applied [28]. Signal processing techniques are utilized for handling a pileup using a combination of hardware and software

Table 1 Research progress on overcoming a pileup

Algorithms	Challenges
Trapezoidal filter algorithm [17]	Optimal selection of trapezoidal parameters is needed
True pulse shape algorithm [14]	Limited to a counting rate of 68 Kc/s
General pileup function [19]	Limited to lower energy of background
Finite-length deconvolution filters [20]	Complex structure and accuracy limited to 93%
Modified phase-only correlation [21]	Shows much higher complexity and computational cost
Pulse clipping algorithms [21]	Limited to accuracy and information loss

architectures [29]. A nuclear pulse generator developed through the MATLAB environment has been designed for simulating SOP alpha peaks. SOP algorithms have been presented to handle this issue. In addition, optimum peak detection through an optimization algorithm is a concern. Such optimization algorithms have been developed for the retrieval of optimum peaks, and ALO and PSO algorithms have been adapted for this purpose. The remainder of this paper is constructed into six sections. The developed peak retrieving algorithms are described in Sect. 2. The ALO principles are specified in Sect. 3, and the optimized retrieval of the SOP alpha peak using the PSO is detailed in Sect. 4. The observable results are then described in Sect. 5. Finally, some concluding remarks regarding the prepared algorithms are provided in Sect. 6.

2 Advanced retrieval algorithms of SOP alpha peaks

2.1 Retrieval of SOP alpha peaks based on pulse decomposition

The recorded differential pulse height spectrum for an alpha radiation detector is equivalent to the convolution of the distributed energy of the alpha radiation with a response function of a radiation detector. A deconvolution is the inverse process and represents the decomposition of overlapped peaks into separate components using various techniques. The SOP peaks from the scintillator detector are an essential issue of alpha spectroscopy applications. The SOP peak represents a major challenge within spectroscopy applications. The SOP causes a direct counting loss. The interval distribution of the emitted radiation particles is as follows [15]:

$$\psi(\delta t)\mathrm{d}t = \alpha_n e^{-\alpha_n \delta t}\mathrm{d}t, \tag{1}$$

where α_n, t, and δt represent the actual average rate of the alpha radiation, stamping of the existing time pulse, and the proportional center of the time axis, with a considerably smaller interval time within δt and $\delta t + \mathrm{d}t$, respectively. The energy resolution of the spectrum obtained is improved through the collection of the light time. The avoidance of an SOP pulse within a series of pulses yields the following probability:

$$p(\delta t > \tau) = \exp(-\alpha_n \tau), \tag{2}$$

where τ denotes the initial pulse width. The probabilities of the SOP for the true counting rate can be demonstrated through Eq. (2), as shown in Fig. 1. The SOP probability decreases with a reduction in the pulse width. It can be seen that the SOP is influenced by the width of the alpha radiation pulse and the emission rate of the alpha radiation

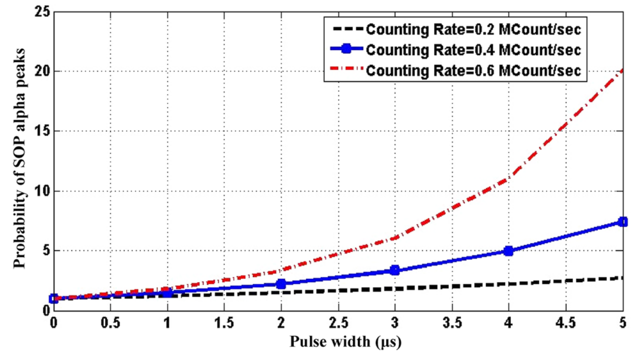

Fig. 1 Probability of SOP against pulse width for different counting rates of alpha radiation sources

source. The excitations and deexcitations at the activator sites are accompanied with the decay time. Thus, multiple decay times exist with various components. The decay time of NaI(TI) is approximately 230 s [16]. Thus, a shaping circuitry is essential for controlling the trailing edge of the alpha peak within approximately 200 s [30]. However, it is lower than 1 s for faster inorganic materials such as BaF_2 [16]. Moreover, the decay time may be longer owing to secondary deexcitations [16]. This process is responsible for the pulse formation [16]. Finally, the decay time constant for anthracene as an organic scintillator was found to be 3.68 s [16]. In addition, the output of the amplifier is often between 0 and 10 V [16]. The amplifier is used for shaping the tail pulses at the output of the preamplifier. It converts the tail pulse to a linear amplified pulse within this specified voltage range. The peak positions are affected by two factors, namely the resolving time and the counting rate. The positions of overlapping peaks depend on the resolving time of the detector, which is the minimum time for separating adjacent pulses [15]. Moreover, the counting rate is another significant parameter that changes the pulse position. Four different algorithms are also proposed, namely the peak seek, slope tangent, fast array, and average combinational algorithms. The specifications of such algorithms are described below.

2.2 Proposed SOP retrieving algorithms of digital alpha spectroscopy

This subsection describes an evaluation of the four different proposed algorithms for resolving SOP alpha peaks. An algorithm for the signal separation and retrieval of alpha peaks depending on the peak seek method is proposed. This algorithm is tested using SOP alpha peaks. The alpha peaks are corrupted by white Gaussian noise (WGN). The accuracy of the algorithm is estimated under various noises. The peak seek algorithm is implemented in Fig. 2. This algorithm has strength in that it handles ties between

Fig. 2 Retrieval of SOP alpha peaks using peak seek algorithm

Step 1: **Initialize Gaussian Pulse Parameters Including {Amplitude, Width, and Position} [16]**
Step 2: **Generate a SOP Alpha Peaks**
Step 3: **Apply Peak Seek for Estimating Peak Heights**
- **Read and Input All Detected Pulses**
- **Do Comparison between Adjacent Points to Find Peaks That Satisfy Previous Point<Peak< Next Point**
- **The Minimum Distance between Peaks is Assumed as Unity on X-Axis if not Specified**
- **If Minimum Distance between Peaks >1 then Do the Following**
- **Initialize the Value of Minimum Detected Peak Amplitude**
- **Find Location of All Maxima and Ties of This Pulse**
- **Determine Difference Between Adjacent Points for Pulse Location**
- **Compare Minimum Peak Distance with Differentiation of Vector Location**
- **Find Values in the Vector at Zero Locations**
- **Estimate the Amplitude Corresponding to these Location Points**

Step 4: **Estimate the Values of Original Peaks Parameters {Amplitude, Position, and Width}**
Step 5: **Draw Isolated Gaussian Peaks Using Retrieved Pulse Parameters {Amplitude, Width, and Position}**
Step 6: **Detect False Peaks**
Step 7: **Compare Sum of Retrieved Peaks with Original SOP Peaks**
Step 8: **Guess the Error Peak Parameters**

neighboring peaks. With this algorithm, the minimum peak height is initiated. The detected peak should fulfill such a constraint. Otherwise, the peak is erased. In addition, this algorithm deals with the required minimum distance between peaks, and is used with the minimum height of the peaks. The peak height is obtained through a comparison between adjacent points, and is located between the previous and forward peaks. Hence, the estimated peak should satisfy the following criterion:

$$P_r < \text{Peak} < S_u, \tag{3}$$

where P_r and S_u are the preceding and successive peak points, respectively. The locations of these peaks are approximated within the minimum distance between neighboring peaks, and as unity along the time axis unless otherwise specified. In such a case, the interval between neighboring points is considered to be fixed. If not, the least distance between peaks is presumed and applied. The location of the maximum points is then estimated. The difference between any two adjacent points is obtained ($V_{k-1} < V_k < V_{k+1}$), which represents the slope of the corresponding signal points. Consequently, the slope of the alpha pulse is given as follows [31]:

$$\frac{dV}{dt} = \frac{V_{k+1} - V_k}{\xi_{k+1} - \xi_k}, \tag{4}$$

where ξ denotes the time values for the kth points of the derivative, and

$$\frac{d\xi}{dt} = \left.\frac{(\xi_{k+1} + \xi_k)}{2}\right|_{m-1>k>1}, \tag{5}$$

where k, m, ξ_k, $\left.\frac{d\xi}{dt}\right|_k$, and $\left.\frac{dV}{dt}\right|_k$ indicate sample corresponding to each V_k or ξ_k, the number of points within the alpha peak, the corresponding time, and the voltage for the number of points of the tangent peak, respectively. The values obtained from the slope are compared with the estimated peak distance. The zero values in the expected vector correspond to the peak location. Thus, the positions of all peaks are estimated, and the peak parameters (amplitude, position, and width) are found using the peak seek algorithm. The shape of the reconstructed pulse resembles a Gaussian pulse because the alpha pulses are approximated as having a Gaussian shape. The components of the original peaks are estimated as illustrated in Step 4 of Fig. 2. These components restore the original shape of the peaks. The peaks retrieved should be checked to avoid deceptive peaks. Otherwise, these peaks are passed to the spectroscopy system. An error in the restored peaks is attained for an evaluation of such an algorithm.

Another algorithm is proposed to resolve and decompose a set of overlapping peaks into their separate components. The slope tangent algorithm is employed for this target, as specified in Fig. 3. This proposed algorithm is utilized for estimating the peak heights and position. These detected peaks and position are applied in several dependent steps. The difference between the closest events may be applied for facilitating the retrieval of SOP alpha peaks. These retrieved peaks are converted into their separate components. In addition, these peaks are approximated into Gaussian peaks. The difference involving neighboring events looks to be identical to the slope of the tangent of the alpha signal. The slope tangent algorithm is described using a spectral discrimination property. The intervals between neighbor points in an alpha radiation signal are considered to be fixed (ΔV = constant). Equations (4) and (5) are utilized for computing the slope of the tangent. The zero points are estimated. These points correspond to the location of maximum peaks. Moreover, the slope of the tangent for these points is estimated. This refers to a bending within the alpha radiation signal. In other words, it corresponds to the changeable rate of the alpha signal, and is computed as follows:

Fig. 3 Retrieved peaks from SOP alpha signals using slope tangent algorithm

Step 1: Initialize Gaussian Pulse Parameters Including {Amplitude, Width, and Position} [16]
Step 2: Generate SOP Alpha Peaks
Step 3: Conduct Peak Search
- Estimate Difference between Neighbor Points (D)
- Find Intersection with Zero Values with X-Axis
- Do Differentiation for obtained Values of D
- Find Peak Values that <0
- Find Location of Peaks that >0

Step 4: Retrieve Original Piled up Peaks
Step 5: Draw Isolated Gaussian Peaks Using Retrieved Pulse Parameters {Amplitude, Width, and Position}
Step 6: Detect False Peaks
Step 7: Compare Sum of Retrieved Peaks with Original SOP Peaks
Step 8: Guess the Error Peak Parameters

$$\frac{d^2V}{dt^2} = \frac{V_{k+1} - 2V_k + V_{k-1}}{\Delta\xi^2}, \tag{6}$$

$$\frac{d\xi}{dt} = \xi_k|_{m-1>k>2}. \tag{7}$$

Owing to the linearity of such a method, the retrieved peaks from the SOP should correspond to the original peaks. The result obtained can be either positive or negative. The maximum peaks correspond to concave edges with negative values.

A third proposed peak recovery algorithm is employed for an estimation of the original peak components. This algorithm is designated as a fast array algorithm, as shown in Fig. 4. This algorithm searches the locations of the maxima points within the radiation vector. In addition, it finds the corresponding maximum values in a 1D array. The length of the alpha radiation signal is initialized. The two end points are excluded from this vector. Subsequently, a vector of the local maxima is created. This vector begins and ends with zero points because the start and end points are excluded from the radiation vector. A signum function is utilized for a comparison regarding the adjoining points. Unity is returned if the difference in the neighboring events is greater than unity. Otherwise, a zero value is returned. Thus, the local maximum equivalent to unity is given as follows:

$$P = \Im(\Im(S_{2:N+1} - S_{3:N+2}) - \Im(S_{1:N} - S_{2:N+1})) + 1, \tag{8}$$

where $\Im$, S, and N are the signum function, vector of the alpha signal, and end point of the alpha signal excluding the max edge points, respectively. The signum is identical to a sign function and applies an element-by-element vector. The subtraction of shifted vectors is equivalent to the difference between adjacent points. The output of the preceding formula will be +1 for the local maxima, − 1 for the local minima, and 0, otherwise, and is basically indicated as follows:

$$P = \begin{cases} +1 & \text{Maximum} \\ -1 & \text{Minimum} \\ 0 & \text{Elsewhere} \end{cases}. \tag{9}$$

Logical values of the maxima are then estimated. A binary form of zeros and 1 s is obtained, and indices of the maximum values are introduced that determine the maximum values. These values are proportional to the peak amplitude. This algorithm returns a 2 N array with peak heights and positions. The estimated peak amplitude and position of the SOP peaks are applied to the Gaussian shape. Thus, the reconstruction and recovery of the original peaks are investigated. Overcoming the false pulses is essential. Thus, the accuracy of such an algorithm is compared with other proposed retrieval algorithms.

The final algorithm is shown in Fig. 5. This algorithm relies on a combination of the three proposed algorithms

Fig. 4 Retrieved peaks from SOP alpha signals using fast array search algorithm

Step 1: Initialize Gaussian Pulse Parameters Including {Amplitude, Width, and Position} [16]
Step 2: Generate a SOP Alpha Peaks
Step 3: Do Fast Array Peak Finder
- Find Locations of Local Maxima
- Estimate Length of Input Vector and Exclude End Point Maxima
- Apply Signum Function for Comparison between Signal Points

$$P = \Im\left(\Im\left(S_{2:N+1} - S_{3:N+2}\right) - \Im\left(S_{1:N} - S_{2:N+1}\right)\right) + 1$$

- Signum of Unity Value Corresponds to Maxima, and 0, Otherwise
- Convert Numeric Values of Local Maxima to Logical
- Estimate Indices of Maxima and Corresponding Values of Input Pulse
- Find value at Maximum Corresponding to Peak Amplitude
- Find Index Value for Maximum Corresponding to Peak Location

Step 4: Estimate Peak Parameters Including {Amplitudes, Widths, and Positions}
Step 5: Draw Individual Gaussian Peaks Using Retrieved Pulse Parameters {Amplitude, Width, and Position}
Step 6: Detect False Peaks
Step 7: Compare Sum of Retrieved Peaks with Original SOP Peaks
Step 8: Guess the Error Peak Parameters

Fig. 5 Retrieved peaks from SOP alpha signals using average combinational algorithm

Step 1:	Initialize Gaussian Pulse Parameters Including {Amplitude, Width and Position} [16]
Step 2:	Generate a SOP Alpha Peaks
Step 3:	Obtain Height and Position of Each Peak Using ○ Peak Seek Search ○ Peak Search By Slope Tangent ○ Fast Array Peak Finder
Step 4:	Compute Average of Estimated Peak Heights
Step 5:	Obtain Average of Deduced Peak Positions
Step 6:	Estimate Peak Parameters Including {Amplitudes, Widths, and Positions}
Step 7:	Draw Individual Gaussian Peaks Using Retrieved Pulse Parameters {Amplitude, Width, and Position}
Step 8:	Detect False Peaks
Step 9:	Compare Sum of Retrieved Peaks with Original SOP Peaks
Step 10:	Guess Error Peak Parameters

(peek seek, slope tangent, and fast array algorithms). Thus, it is a called the average combinational algorithm. This algorithm depends on the peak values extracted from the other three algorithms. A register is then opened for storing the average extracted amplitude. Subsequently, the positions of the maximum peak heights are captured. These values are averaged. The alpha peak heights are retrieved by calling the stored maximum heights and corresponding positions. A reconstruction of the original alpha peaks is applied. Similarly, the accuracy of this algorithm is compared. The proposed algorithms show several advantages regarding the retrieval of SOP alpha peaks. These merits include robustness against noise attacks, a higher processing time, simplicity, and accuracy. In addition, these algorithms can be modified for the retrieval of a high-order pileup of the alpha peaks.

3 Optimum SOP peak retrieval in alpha spectroscopy using ALO algorithm

3.1 ALO preliminary

The ALO is a nature-inspired algorithm. This algorithm resembles the natural hunting process of antlions. The ALO algorithm shows several advantages in dealing with optimization issues of signal processing applications, as stated in [32], namely a local optima avoidance, derivation independency, simplicity, and problem independency [33]. The consumable time of the ALO is the main drawback that should be dealt with, which is due to the random walk (RW) process [32]. The hunting prey process includes five different steps, as shown in Fig. 6 [33]. RWs correspond to ant movement [32–34]. This is the initial step, and consequently, traps are created. Thus, the entrapment process for ants in a trap is considered and the catching of prey is applied. Traps are then rebuilt for an additional process. This algorithm is used to find the superior optimum peak parameters of the SOP peaks within the alpha spectroscopy.

This optimization algorithm stimulates the process of interaction between antlions and ants within the traps. Thus, it is essential for ants to be moved over the search space to model and express this interaction. Antlions are permitted to hunt their prey and become fitter through traps. In nature, ants move randomly when searching for food. Thus, an RW is selected to describe the movement of ants. A matrix is created for saving and expressing the optimum positions of the ants. This matrix is illustrated as follows [33, 34]:

$$T_{\text{Ant}} = \begin{bmatrix} M_{1,1} & M_{1,2} & \cdots & \cdots & M_{1,d} \\ M_{2,1} & M_{2,2} & \cdots & \cdots & M_{2,d} \\ \cdots & \cdots & \cdots & \cdots & \cdots \\ M_{n,1} & M_{n,2} & \cdots & \cdots & M_{n,d} \end{bmatrix}, \tag{10}$$

where T_{Ant}, $M_{i,j}$, n, and d indicate the matrix employed for saving the positions of all ants, the value of the jth variable of the ith ant, the numbers of ants, and the corresponding number of variables, respectively. These antlions are considered to be hiding within the search space. A matrix is constructed to save their fitness function as follows [33, 34]:

$$T_{\text{OAL}} = \begin{bmatrix} f(AO_{1,1}, AO_{1,2}, \ldots, AO_{1,d}) \\ f(AO_{2,1}, AO_{2,2}, \ldots, AO_{2,d}) \\ \cdots \\ f(AO_{n,1}, AO_{n,2}, \ldots, AO_{n,d}) \end{bmatrix}, \tag{11}$$

where $AO_{i,j}$, n, and f denote the jth dimensional value of the ith antlion, number of antlions, and the objective function, respectively. The optimization procedure contains six fundamental steps.

The first step is indicated for the RWs of the ants. The movement of the ants is stochastic. Thus, a random walk is used to model the movement of the ants as follows [33]:

Fig. 6 Hunting prey steps depending on ALO algorithm

$$\psi(t) = [0, \mathrm{Cum}(2r(t_1) - 1), \ldots, \mathrm{Cum}(2r(t_n) - 1)], \quad (12)$$

where Cum, n, t, and $r(t)$ indicate the cumulative sum, largest number of iterations, steps of an RW, and a stochastic function of 1 (rand > 0.5) or 0 (rand ≤ 0), respectively. An updating of the position of the ants is conducted at every step of an RW. The ants should apply the search space within specific boundaries. The min–max normalization procedure is utilized to maintain a stochastic walk within the search space as follows [33, 34]:

$$Z_i^t = \eta_i^t + \frac{(z_i^t - \lambda_i)(d_i - \eta_i^t)}{\gamma_i^t - \lambda_i}, \quad (13)$$

where λ_i, γ_i, η_i^t, and Θ_i^t denote the least RW of the ith variable, the max RW in the ith variable, the lowest ith variable at the tth iteration, and the maximum ith variable at the tth iteration, respectively. This formula guarantees the existence of an RW within the search space. Thus, this formula is applied with any iteration.

The second step is trapping within the antlion pits. Traps have a significant influence on the RWs, which are modeled as follows [33]:

$$\begin{cases} \eta_i^t = \eta^t + \mathrm{Antlion}_j^t \\ \Theta_i^t = \Theta^t + \mathrm{Antlion}_j^t \end{cases}, \quad (14)$$

where η^t, Θ^t, and $\mathrm{Antlion}_i^t$ denote the minimum of all variables at the tth iteration, the vector including the maximum of all variables at the tth iteration, and the position of the preferred jth antlion at the tth iteration, respectively. This performance is described through Fig. 7. A 2D search space is needed by the ants to move within the hypersphere around the antlions.

The third step is the creation of traps. The hunting process of antlions is declared using a roulette wheel. As a result, roulette wheel operative is functionalized through the ALO for picking appropriate antlions. A roulette wheel can be considered for the capturing factors from a finite set, which are weighted using 1/fitness. This selection is based on the fitness mechanism. Thus, a fitter antlion will have a chance to catch an ant.

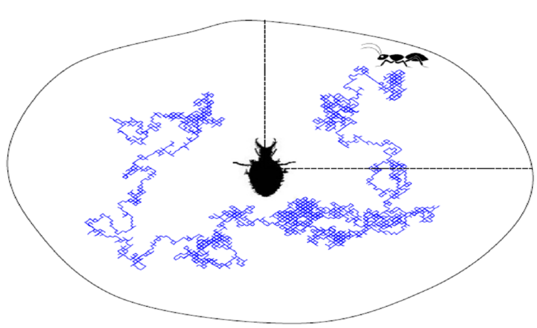

Fig. 7 RW for ant in a trap [33] (Color online)

The fourth step is the sliding of ants in the direction of the antlions. The antlions build a trap randomly for ants relative to their fitness. Thus, the antlions place sand outside the pit if the ant enters the trap. Thus, the ant is moved slowly down within the trap. Thus, numerous trials by the ant to escape the trap are carried out. The RW hypersphere has a decreased radius. This behavior is modeled as follows [33]:

$$\begin{cases} \eta^t = \dfrac{\eta^t}{I} \\ \Theta^t = \dfrac{\Theta^t}{I} \end{cases}, \quad (15)$$

where I denotes the ratio, the minimum of all variables at the tth iteration, and a vector including the maximum of all variables at the tth iteration, respectively. The previous expressions shrink the radius of the ant positions. In addition, these formulas resemble the sliding of the ant within the pit. This is essential to continue the search within the search space.

The fifth step is catching prey and re-building the pit. Finally, the antlion catches the ant within its jaws when the ant reaches the bottom edge of the pit. The ant is pulled inside the sand by the antlion, which consumes the ant's entire body. It is necessary to repeat this process for new prey. Thus, the positions of the antlions are updated for increasing the probability of catching new prey. These processes are formulated as follows [33]:

$$\mathrm{Antlion}_j^t = \mathrm{Ant}_j^t \text{ if } f(\mathrm{Ant}_j^t) > f(\mathrm{Antlion}_j^t), \quad (16)$$

where t, $\mathrm{Antlion}_j^t$, and Ant_j^t denote the current iteration, position of the selected jth antlion at the tth iteration, and the position of the ith ant at the tth iteration, respectively.

The final sixth step is specified for elitism. This is the most fundamental property of the optimization steps in that it achieves the best solution at any stage. This is the optimist antlion. Whole superior antlions are saved inside the elite during any iteration, which affects the ant movement. Ants as RWs behind the chosen antlion for both the roulette wheel and the elite antlion are written as follows:

$$\mathrm{Ant}_i^t = \frac{1}{2}(\Delta_A^t + \Delta_E^t), \quad (17)$$

where Δ_A^t, Δ_E^t, and Ant_i^t denote an RW around an antlion selected by the roulette wheel at the tth iteration, an RW behind elite at the tth iteration, and the position of the ith ant at the tth iteration, respectively.

3.2 Optimum detection of SOP alpha peaks using the ALO algorithm

The ALO optimization algorithm can be applied to the optimum detection of alpha peaks, as indicated in Fig. 8.

Fig. 8 Pseudo-code of antlion optimizer algorithm for overcoming SOP peaks of digital alpha spectroscopy

```
Step 1:  Perform Signal Separation and Recovery using Retrieving Algorithm
Step 2:  Initialize the Number of Search Agents and Maximum Number of Iterations
Step 3:  Read Sum of Retrieved Peaks Using
            o  Peak Seek Algorithm
            o  Slope Tangent Algorithm
            o  Fast Array Algorithm
Step 4:  Apply Antlion Optimizer (ALO) Search
            o  Initialize Position of Antlions
            o  Initialize Variables to Save Position of Elite, Convergence Curve, Antlions Fitness
            o  Calculate Fitness of Initial Antlions and Sort Them
            o  While (Iter<Max+1), First iteration is Considered for Computing Fitness of Antlions
            o  Apply 'for' Loop to Simulate Random Walks
            o  Determine Random Walk around the Selected Antlion by Rolette Wheel
            o  Get Random Walk around the Elite (Best Antlion)
            o  Apply Boundary Checking and Bring Back Antlions Inside Search Space As
         They>Boundaries
            o  Update Antlions Positions and Fitness based on Ants
            o  Updated Antlion Goes to Its Position to Build Trap if Ant is Fitter than Antlion
            o  Update the Position of Elite Antlion if Any Antlion Becomes Fitter than It
            o  Keep the Elite Antlion in Population
            o  Update the Convergence Curve
Step 5:     o  Display both Iteration and Best Optimum Values
         Obtain Best Position, Score, and Convergence Curve
```

This algorithm depends on the proceeding steps for a localization of the maximum peaks. The operational principle of this algorithm is discussed and presented in [33]. This algorithm can be approximated through three-tuple functions. These functions express the global optimum for the optimization problems as follows:

$$\mathrm{ALO}(X, Y, Z), \tag{18}$$

where X, Y, and Z are functions that introduce random initial solutions, manipulate the initial population supplied by function X, and return a true value when the end criterion is met, respectively. The input SOP peak is handled using one of the proposed signal recovery algorithms. An SOP retrieving algorithm, i.e., the peak seek, slope tangent, or fast array algorithm, is selected. Subsequently, the inputs to the ALO algorithm are the sum of the recovered peaks for checking the accuracy of the proposed algorithm. In addition, the algorithm attempts to find the optimum positions for the maximization requirements.

The matrices of the antlion and ant are randomly initialized using the sum of nonlinear recovered peaks of the selected peak recovery algorithm. The position of an ant is updated in proportion to the chosen antlion through the roulette wheel and elite antlion. The boundary positions are updated using the maximum number of iterations. This is demonstrated through the RWs around the simultaneously selected antlion and elite antlion [33]. The RW of the ants is measured in terms of the fitness function. Therefore, the estimated position behaves as a fresh function for the antlion of the next generation if the ants are fitter than the antlion. The antlion performances are compared. This process is repeated if function Z returns a false value. Thus, a convergence curve is displayed. This curve shows the best optimum values with their iterations. The optimum positions are determined. The evaluation metrics of such an algorithm are also investigated. In addition, the ALO and PSO techniques are functionalized for evaluating the accuracy of the peak retrieval algorithms. However, they are linked to one of the peak retrieval algorithms. Thus, the operational principle and relation between the ALO and PSO optimization algorithms linked to the peak retrieval algorithms are presented in Fig. 9. The proposed optimum peak retrieval algorithms are new and have not been mentioned before. They have the advantage of dealing with nonlinear [35] alpha peaks. The ALO/PSO algorithms can deal with high counting rates of the alpha peaks. Gradient

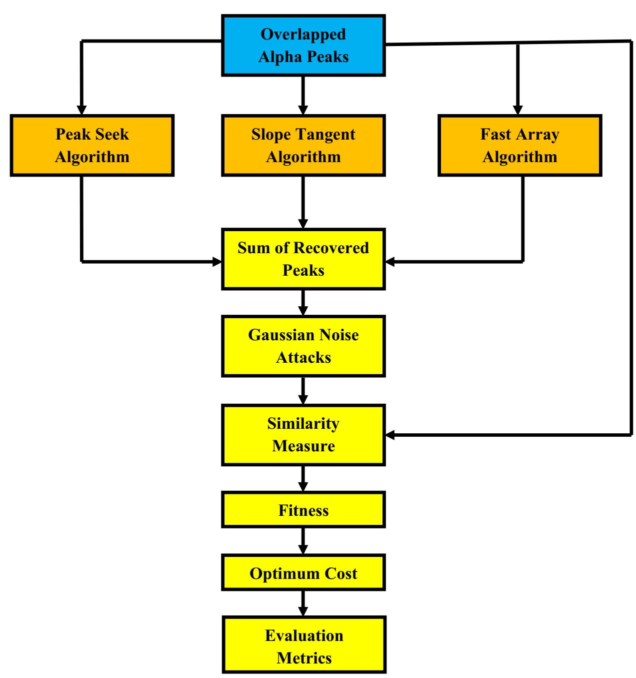

Fig. 9 Proposed optimum peak detection of SOP alpha ray spectroscopy using ALO and PSO algorithms

information for the coming unknown function is not necessary [35]. No explicit formulas are needed for objective functions. This is restricted to the functional value of the wanted objective function [35].

4 Optimum SOP Peak Retrieval in Alpha Spectroscopy using PSO Algorithm

The PSO is approximated as an evolutionary computation method. This technique is incorporated within the field of swarm intelligence. In 1995, Eberhart and Kennedy explored the idea behind the PSO [36, 37]. The PSO includes a wide diversity of swarms and flying directions, the importance of the exploration space, and searching methods [35]. In addition, the search process is located in the direction of the greatest fitness [35]. The PSO is accompanied with an inclusive class of populated stochastic optimization [35]. As a result, it resembles an iterative algorithm [38]. The PSO is based on populated individuals defined as particles [38]. The primary population is randomly distributed within the search space as a suggested solution [36, 37]. In the PSO, every particle has a velocity and position, called a solution vector. Subsequently, the best solution of the PSO is maintained in memory. This solution looks like a vector, which is attained by all candidate solutions within the search space [36, 37]. The PSO algorithm for handling SOP peaks of digital alpha spectroscopy is shown in Fig. 10. This figure illustrates the principle of the PSO for a deconvolution of the SOP alpha peaks. The algorithm is summarized in Fig. 10, and described in the following sections. Besides, the operational principle of PSO is declared in Fig. 11.

The initial step is swarm initialization. A solution vector (Δ) is assigned to each particle as a primary step. It contains μ parameters specified by $\Sigma_1, \Sigma_2, \ldots, \Sigma_\mu$, and is related to the jth candidate solution. This vector is a function of the μ element in the rows [35–37].

$$\Delta_j = \left[\Sigma_1, \Sigma_2, \ldots, \Sigma_\mu\right], \tag{19}$$

where Σ defines the solution vector of the jth candidate solution. Subsequently, the PSO code is applied [35] to optimize the peak height of the recovered peaks of the alpha signals within the alpha ray spectroscopy. The first class of individuals can be created randomly in an interval between 0 and 1 of Σ. Next, the velocity and solution vector are updated [39]. It is important to update the velocity and candidate solution during $t + 1$ iterations as follows [36, 37]:

$$S_{ij}(t+1) = \psi \cdot S_{ij}(t) + \chi_1 \cdot f_1 \cdot (pbest_i(t) - \Sigma_{ij}(t)) + \chi_2 \cdot f_2 \cdot (gbest(t) - \Sigma_{ij}(t)) \tag{20}$$

where *pbest* is a personnel learning parameter, and *gbest* denotes the global training parameter.

$$\Sigma_{ij}(t+1) = \Sigma_{ij}(t) + S(t+1), \tag{21}$$

where S_{ij} denotes the velocity and jth dimension of the ith candidate solution, respectively, and χ_1 and χ_2 are the acceleration constants. The parameter ψ is the inertia weight. Chaotic inertia [39] is related to the local and global searches of the PSO. Its weight is applied to restore the SOP alpha peaks using the PSO. A chaotic mapping is applied to set the inertia weight coefficient. These constants are predefined by the user. The parameters f_1 and f_2

Fig. 10 PSO algorithm for overcoming SOP peaks of digital alpha spectroscopy

Step 1: **Obtain the Output of Proposed Alpha Retrieval Algorithms**
- **Peak Seek Algorithm, Slope Tangent Algorithm, and Fast Array Algorithm**

Step 2: **Sum the Retrieved Peaks**

Step 3: **Define Each of the following**
- **Number of Decision Variables and Size of Decision Variables**
- **Lower Bound of Variables and Upper Bound of Variables**
- **Maximum Number of Iterations**
- **Population Size or Swarm Size**
- **Inertia Weight and Inertia Weight Damping Ratio**
- **Personal Learning Coefficient and Global Learning Coefficient**
- **Velocity Limits**

Step 4: **Initialize Each of the Following**
- **Position and Velocity**

Step 5: **Update Each of the Following**
- **Personal Best (Pbest) and Global Best (gbest)**

Step 6: **Perform Main 'for' Loop of PSO with**
- **Update Velocity and Apply Velocity Limits**
- **Update Position and Perform Velocity Mirror Effect**
- **Apply Position Limits**
- **Apply Cost Evaluation**
- **Update Personal Best and Update Global Best**

Step 7: **Obtain Optimum Best Cost and Best Position**

Fig. 11 Operational principle of PSO

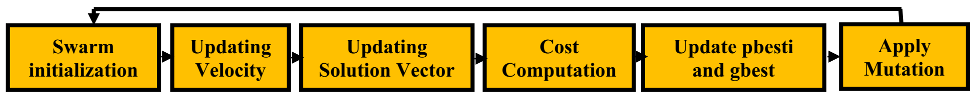

correspond to uniformly created random numbers within the interval between 0 and 1.

The computing cost value ($Cost_i$) of every candidate solution is the necessary third step. Every solution vector includes a cost function. This function creates an output from the solution vector. The cost function can be specified as follows [36, 37]:

$$\text{Cost} = f(\text{solution vector}) = f(\Sigma_1\Sigma_2 \ldots, \Sigma_\mu). \tag{22}$$

The cost function of the PSO can be assessed to find the optimum alpha peak. This function is stated as follows:

$$\text{Cost} = \frac{\left\| \vec{\Omega}_A - \vec{\Omega}_i \right\| + \xi \times \|\beta\|_2}{\left\| \vec{\Omega}_A \right\|_2}, \tag{23}$$

where Ω_A, Ω_i, and ξ represent a vector of the estimated alpha pulse height, a vector of the pulse height spectra obtained by every iteration of the PSO algorithm with the updated Σ, and the mean of the β components, respectively. This is described as follows [36, 37]:

$$N_i = \theta \Sigma, \tag{24}$$

where $\boldsymbol{\theta}$ is a response matrix, the dimensions of which are $n \times m$. The norm 2 of vector $\boldsymbol{S}$ with "n" elements is stated as follows:

$$\|S\|_2 = \sqrt{\sum_{i=1}^{n} S_i^2}. \tag{25}$$

Updating both *pbesti* and *gbest* is the fourth step. A mutation is applied to *gbest* as the fifth step. A mutation to *gbest* is considered when *gbest* does not improve within q updates of *gbest* [40, 41]:

$$gbest_j = gbest_j + \left((\text{cost}(gbest))^l \Big/ \sum_i \sum_j R_{ij} \right) \times \text{Max}(gbest) \times \text{Gaussian}_j, \tag{26}$$

In addition, a mutation is applied to *pbesti* as the sixth step. The mutation to *pbesti* is applied if *pbesti* does not improve within q updates of *pbesti* [40, 41]:

$$pbest_{ij} = pbest_j + \left((\text{cost}(pbest))^l \Big/ \sum_i \sum_j R_{ij} \right) \times \text{Max}(pbest) \times \text{Gaussian}_j, \tag{27}$$

The final step is applying the stopping criteria or repeating the loop. The iteration will continue until reaching the maximized number of generations. However, the stopped state for the PSO algorithm occurs when the best individual is obtained.

5 Results and discussion

Four different algorithms are proposed for the extraction of the SOP peak heights of digital alpha spectroscopy. The retrieved peak positions are tested to avoid illusive peaks. Thus, two basic methods are applied for checking the positions of the retrieved peaks. A conventional method and an optimization approach are employed. The proposed optimization techniques surpass the traditional one, depending on the application of the ALO or PSO algorithm, each of which is linked individually to a peak retrieval algorithm. The deduced results are assessed.

5.1 Recovered peak results of developed algorithms for digital alpha spectroscopy

The results of the peak retrieving algorithms, namely the peak seek, slope tangent, and fast array algorithms, are described in this subsection. The MATLAB environment is considered for the implementation of such algorithms. The simulated SOP peaks of alpha radiation show the influence of these proposed algorithms. The input SOP, retrieved peaks, and sum of the retrieved peaks using the peak seek algorithm are shown in Fig. 12. It should be noted that triple overlapped peaks are discriminated. The pulse parameters are demonstrated by three nonlinear parameters. These parameters are the peak position, peak amplitude, and peak width and are utilized for a reconstruction of the original peaks, which resemble a Gaussian peak shape. In addition, the sum of these retrieved peaks is demonstrated and compared with the input SOP signal. The individual retrieved peaks of the alpha spectroscopy are presented in Fig. 13. These individual peaks can be rejected unless the required condition is satisfied. These peaks are tested as illusive pulses, for which a conventional method is applied. The separation among adjacent pulses has to be larger than half the full width at half maximum (FWHM) of these two pulses. The results show an acceptable peak recovery. Moreover, the accuracy of this algorithm is measured through the parameter expectation and parameter errors (amplitude and positions). The percentage of errors of the estimated peaks parameters is computed as follows:

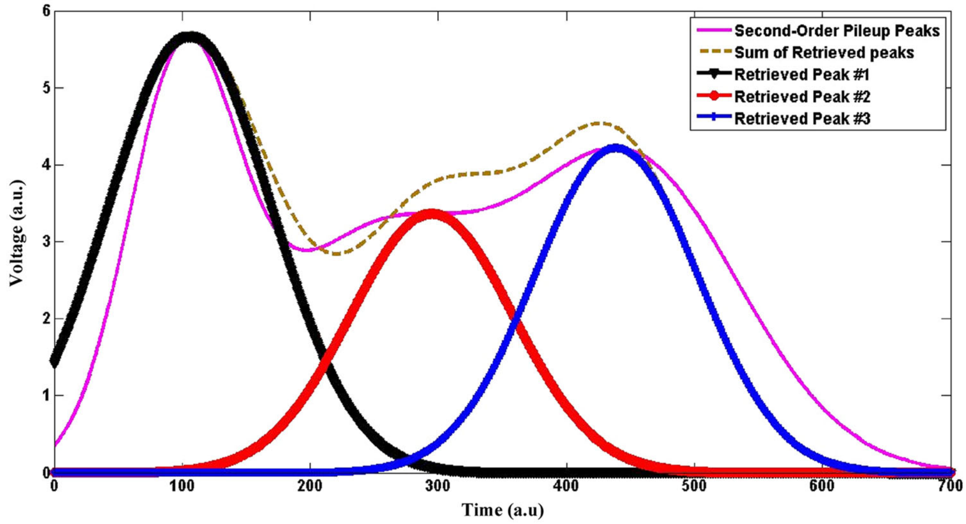

Fig. 12 SOP, sum of retrieved peaks, and individual retrieved peaks using peak seek algorithm (Color online)

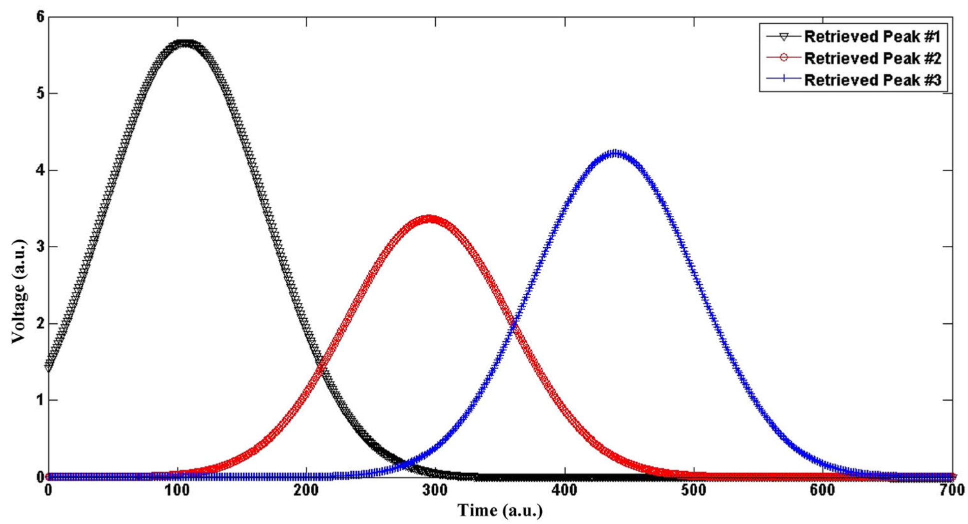

Fig. 13 Separated retrieved peaks using peak seek algorithm (Color online)

$$\xi(M,P) = \frac{A(M,P) - E(M,P)}{A(M,P)}(\%), \tag{28}$$

where E, A, M, and P refer to the estimated peak amplitude, actual input peak, maximum peak, and peak position, respectively. The measured pulse parameters and error of the estimated parameters for overlapping peaks when applying the peak seek algorithm are shown in Table 2. The bases of the initial peak parameter values for all algorithms are shown in Table 2. This table specifies the maximum peak and position values. These values are cited in [16]. The results of the first estimated peak for the maximum peak and peak position are much better than those of the other peaks. In addition, the average error of the recovered peak is 0.0041%, as shown in Table 3. However, the average error of the estimated peak positions is 0.1333%.

The results of the second proposed alpha peak recovery algorithm are presented. This algorithm is used as a slope tangent algorithm. The detected peaks and their corresponding positions are accomplished in successive steps. The detection of the maximum peak heights is realized in Fig. 14. The detection of the maximum peaks depends on the measurement of the difference between adjacent points. The zero value owing to the difference between neighboring points represents the maximum peak. In addition, the separable corrected peaks with a sum of the restored peaks and fresh SOP peaks are introduced in Fig. 15. However, the spited parameters of the SOP peaks owing to the slope tangent algorithm are shown in Fig. 16. Alpha pulses are approximated as having Gaussian shapes when using the estimated nonlinear parameters. These parameters are measured and determined, as shown in Table 2. The errors of such predictable components are also illustrated in Table 2. The negative sign of a component error

Table 2 Measured value and error of estimated parameters for SOP peaks using four proposed algorithms

Algorithms	Estimated parameters	Max. peaks (a.u.)		Positions (a.u.)		Peaks error (%)	Position error (%)
Peak seek algorithm	1st Recovered peak	5.6652	5	106	100	0.0066	0.06
	2nd Recovered peak	3.3640	3	295	250	0.0036	0.45
	3rd Recovered peak	4.2193	4	439	450	0.0021	− 0.11
Slope tangent algorithm	1st Recovered peak	5.6652	5	105	100	0.0067	0.0500
	2nd Recovered peak	3.3640	3	294	250	0.0036	0.4400
	3rd Recovered peak	4.2193	4	438	450	0.0022	− 0.1200
Fast array algorithm	1st Recovered peak	5.6652	5	106	100	0.0067	0.0600
	2nd Recovered peak	3.3640	3	295	250	0.0036	0.4500
	3rd Recovered peak	4.219	4	453	450	0.0731	0.4200
Average combinational algorithm	1st Recovered peak	5.66525	5	105.6667	100	0.006652	0.056667
	2nd Recovered peak	3.3640	3	294.6667	250	0.00364	0.446667
	3rd Recovered peak	4.2193	4	438.6667	450	0.002193	0.113333

Table 3 Average error (%) of recovered nonlinear parameters of SOP alpha signals compared to published experimental algorithms [20, 42]

Algorithms	Average peak error	Average position error
Peak seek algorithm	0.0041	0.1333
Slope tangent algorithm	0.0042	0.1233
Fast array algorithm	0.1092%	0.2200%
Average combinational algorithm	0.1092	0.1682
3-point deconvolution filter [20]	21.486	–
27-point Savitzky–Golay filter [20]	1.506	–
First peak search algorithm in [42]	0.1092	0.1572
Second peak search algorithm in [42]	~0	0.1185

refers to a lower value of the estimated parameter than the actual one. The average error of the maximum peak height is estimated to be 0.0042%, as shown in Table 3. However, the average error of the peak position is found to be 0.1233%. The results of the proposed average combinational algorithm are observed to present results analogous to those of the peak seek algorithm.

The final proposed peak retrieval algorithm relies on a fast array method. The input SOP pulse and detected peak heights using Eq. (8) of the fast array algorithm are presented in Fig. 17. The separated components of the recovered peaks with a sum of the recovered peaks and the original peaks are shown in Fig. 18, whereas the individual recovered triple peaks are illustrated in Fig. 19. From these figures, three nonlinear parameters are attained using the fast array algorithm. A reconstruction of the original radiated peaks from the retrieved peaks is conducted using a Gaussian shape approximation. The parameters of each peak are measured based on the computational error of the estimated parameters, as shown in Table 2. A comparison between the four proposed algorithms with the published experimental algorithms [20, 42] is shown in Table 3. The amplitude errors of the retrieved SOP peaks are 21.486% and 1.506% for the 3-point deconvolution filter and 27-point Savitzky–Golay filter [20], respectively. In addition, the computational average peak and position errors using the implemented peak search algorithm described in [42] are 0.1092 and 0.1572, respectively. Therefore, the peak search algorithm [42] surpasses that found in [20]. For the proposed algorithms, the average error of the deduced maximum amplitude is 0.0204%. In addition, the error of the realized peak position was found to be 0.4867%. The results confirm that the highest retrieved peak is accomplished when using the peak seek algorithm. Moreover, the best recovered peak position is realized by the slope tangent algorithm. However, the worst results are achieved using the fast array algorithm when compared to the results of the other proposed algorithms. So, the compared algorithms demonstrate the best results attained by proposed retrieving algorithms.

5.1.1 Rejection of spurious peaks

There is a minimum distance between any two adjacent peaks for alpha radiation detectors. The occurrence time point represents the leading edge voltage at the threshold.

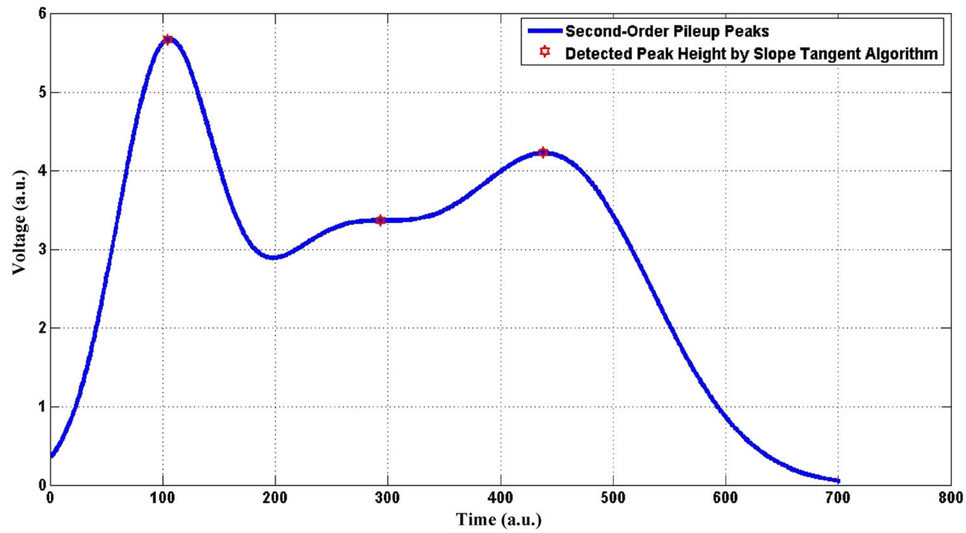

Fig. 14 Maximum detected peaks from SOP peaks using slope tangent algorithm

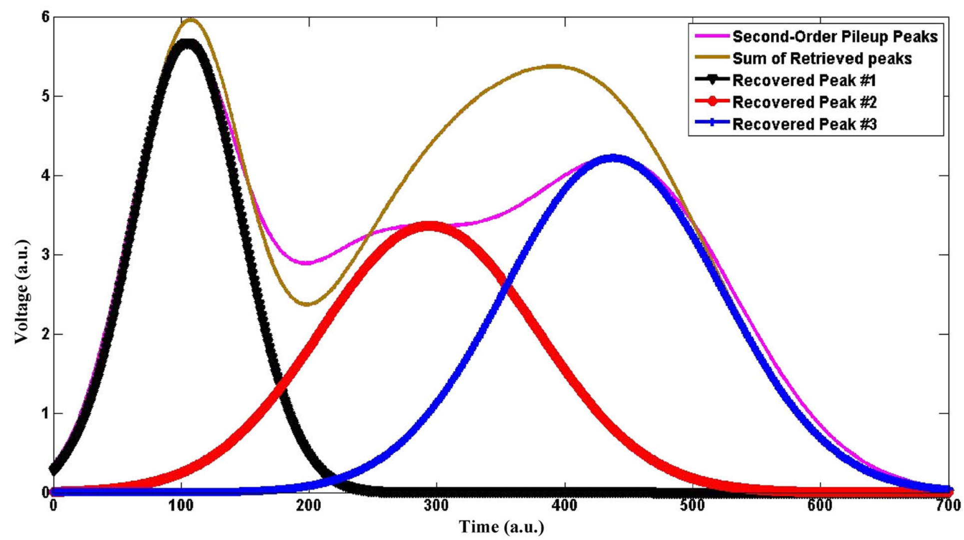

Fig. 15 SOP, sum of retrieved peaks, and separable retrieved peaks using slope tangent algorithm

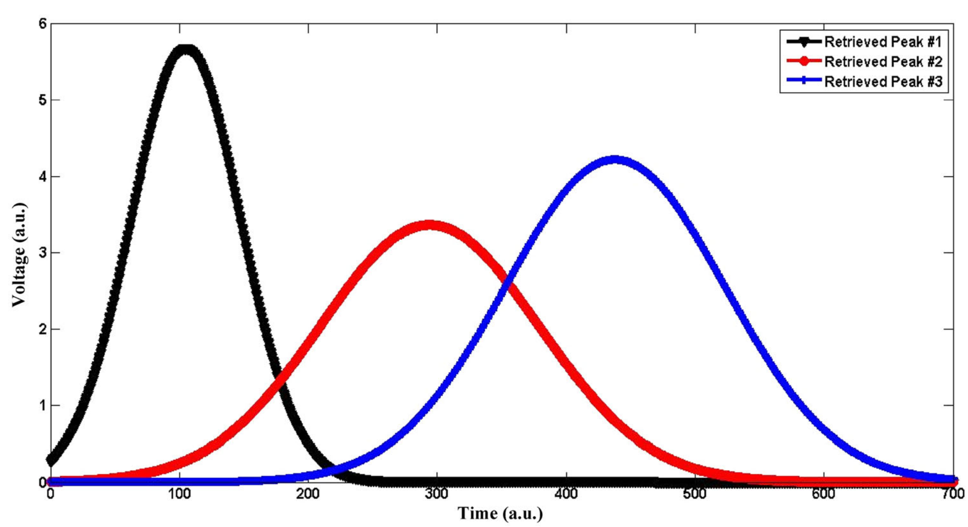

Fig. 16 Isolated retrieved peaks using slope tangent algorithm

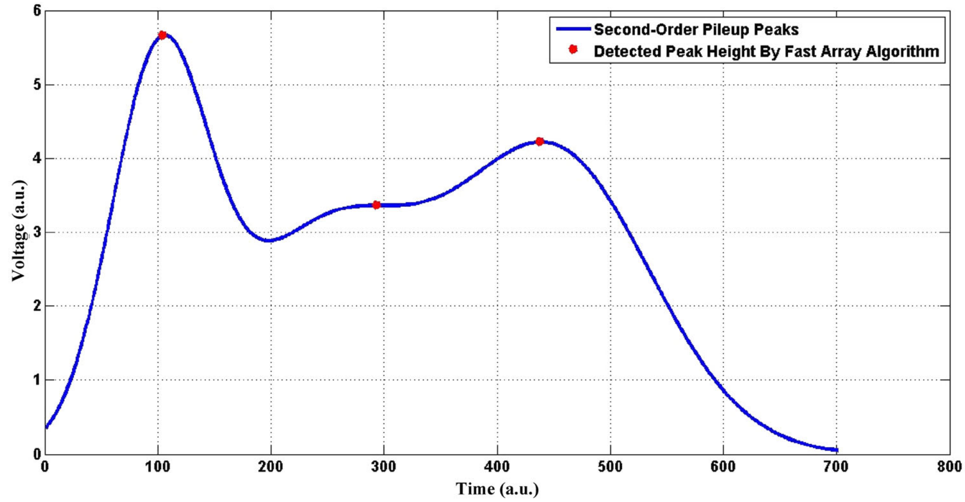

Fig. 17 Maximum detected peaks from SOP peaks using fast array algorithm

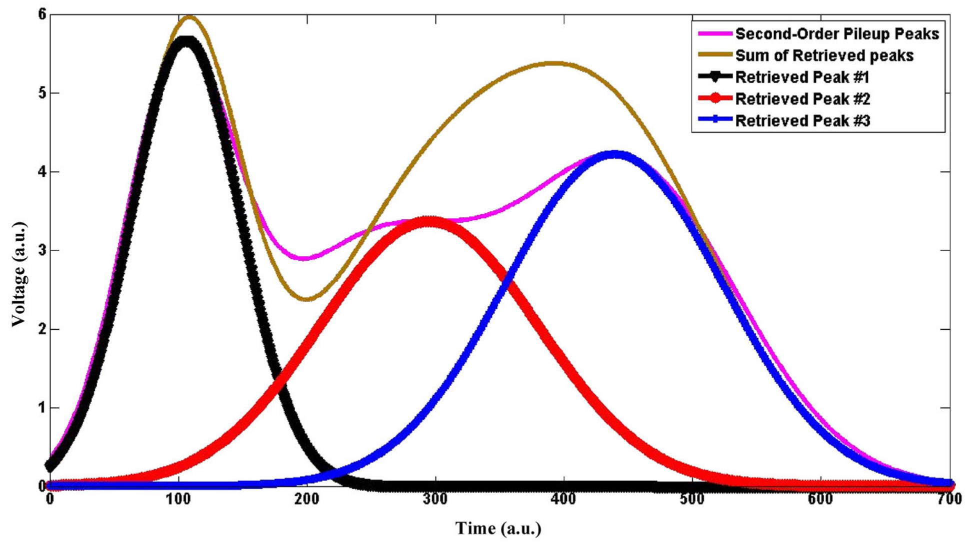

Fig. 18 SOP, sum of retrieved peaks, and separated retrieved peaks using fast array algorithm

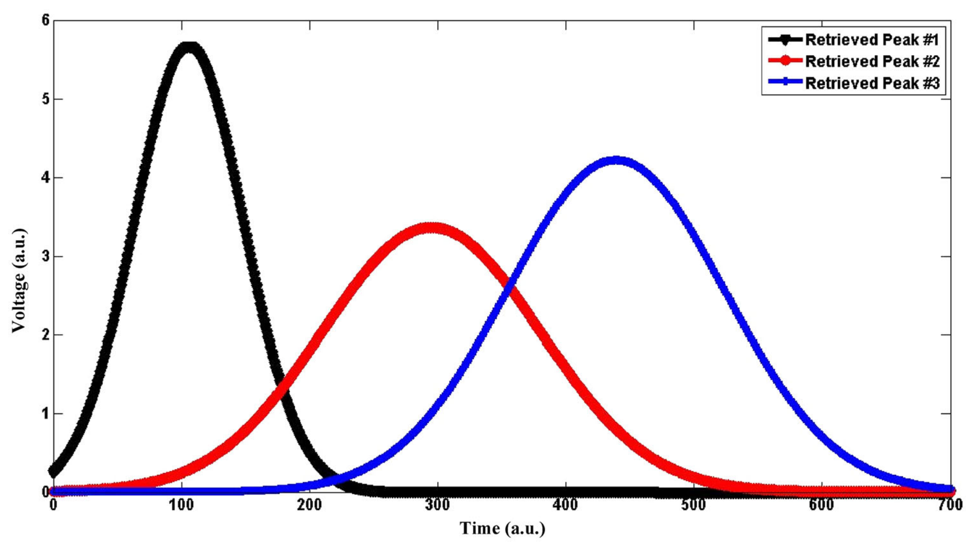

Fig. 19 Separated retrieved peaks using fast array peak algorithm

The SOP within the alpha spectroscopy occurs owing to a lower time interval between the adjacent recovered peaks. This time difference is lower than the pulse width of the first peak. Thus, the interval between adjacent peaks should be higher than the effective pulse width. The output of the retrieved algorithms is registered based on the achievement of this requirement; otherwise, the recovered peak is neglected as being an illusive pulse, and noise removal is desired for handling such pulses. This condition should satisfy the following relation:

$$\Delta T > \begin{cases} \left.\dfrac{\Delta \mathrm{FWHM}_1}{2}\right|_{\text{First \& Second}} \\ \left.\dfrac{\Delta \mathrm{FWHM}_2}{2}\right|_{\text{Second \& Third}} \end{cases}, \tag{29}$$

where ΔT, $\Delta\mathrm{FWHM}_1$, and $\Delta\mathrm{FWHM}_2$ correspond to the difference in the time of occurrence between the first and second peaks and between the second and third peaks, the FWHM distinction between the first and second peaks, and the FWHM difference between the second and third retrieved peaks, respectively. It was observed that the peaks recovered by the proposed algorithms satisfy the previous condition. Thus, the recovered peaks are registered as acceptable for all algorithms.

5.2 Comparison and analysis of the developed algorithms based on ALO and PSO

A comparison between the peak retrieval algorithms of SOP alpha spectroscopy is introduced. In addition, a comparison between the SOP peaks and restored peaks is demonstrated. Accordingly, the calculated error corresponding to the variation between the overlapped peaks and the restored peaks is applied. This error is computed as follows:

$$\Delta\xi = \sum_i \Phi_i - \Theta_i, \tag{30}$$

where Φ_i, Θ_i, and i are the input SOP peaks, sum of the restored peaks, and dataset, respectively. The comparison between the input SOP and the sum of the retrieved alpha peaks shows the accuracy and validity of these algorithms. The differentiation between the sum of the restored peaks and the original input SOP peaks for the peak seek, slope tangent, and fast array algorithms is presented in Figs. 20a, 21, 22a, respectively. The error representing the difference between the sum of the retrieved peaks and the input SOP pulse at all data points is computed by Eq. (30). Such error is investigated in Figs. 20b, 21, 22b for the peak seek, slope tangent, and fast array algorithms, respectively. The

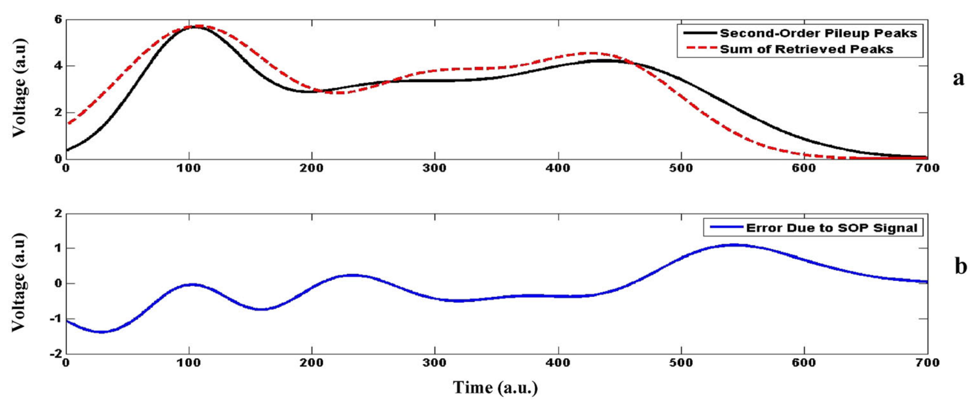

Fig. 20 Accuracy of peak seek algorithm: **a** input SOP peaks and summation of the retrieved peaks and **b** error from SOP peaks

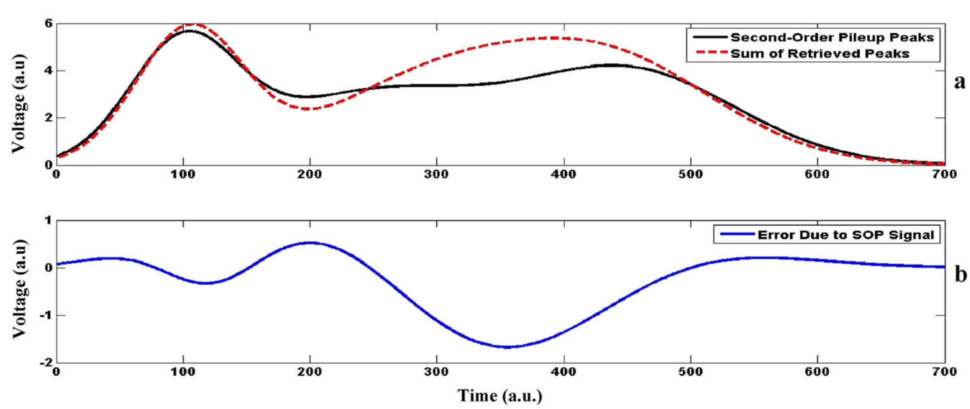

Fig. 21 Accuracy of slope tangent algorithm: **a** input SOP peaks and summation of the retrieved peaks and **b** error from SOP peaks

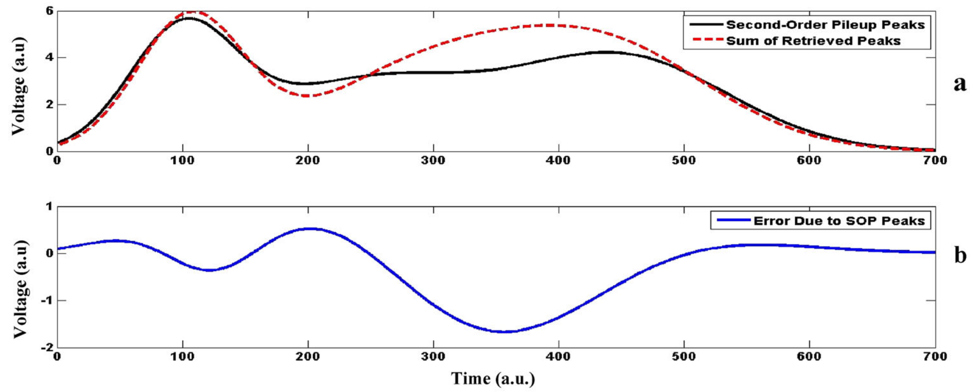

Fig. 22 Accuracy of the fast array peak algorithm: **a** input SOP peaks and summation of retrieved peaks and **b** error from SOP peaks

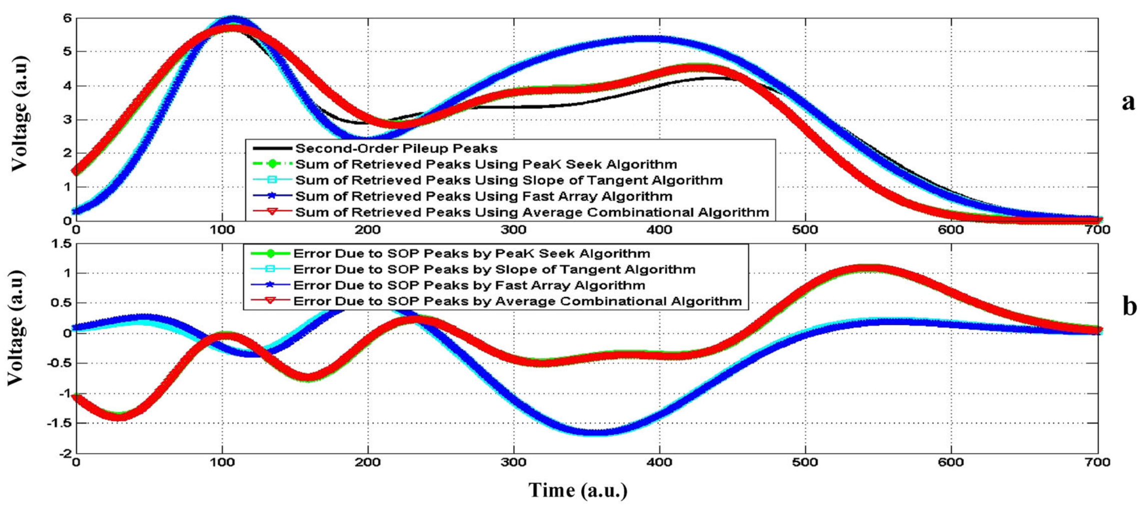

Fig. 23 Accuracy of proposed algorithms: **a** SOP peaks and summation of retrieved peaks for proposed algorithms and **b** error from SOP peaks

Table 4 Estimated parameter errors of proposed peaks retrieving algorithms and experimental published algorithm [42]

Algorithms	Maximum error	Mean error	Height error	Position error	Run time (s)
Peek seek	1.0896	−0.0817	0.1092	0.0719	1.5781
Slope tangent	0.5171	−0.2812	0.1092	0.2146	1.4063
Fast array	0.6100	−0.7129	0.6504	0.2985	1.5000
Average combinational algorithm	1.0992	−0.0810	0.1092	0.1682	2.6676
First peak search algorithm [42]	1.1183	−0.0797	0.1092	0.1572	3.1406
Second peak search algorithm in [42]	3.0249	1.1464	~0	0.1185	2.7656

accuracy of proposed algorithms is summarized in Fig. 23. The input SOP peaks and a summation of the retrieved peaks for the proposed algorithms are shown in Fig. 23a. In addition, the error from the SOP peaks is clarified in Fig. 23b. Qualitative measurements of the proposed and experimental published algorithms are illustrated in Table 4. The peak seek algorithm achieves comparable results to those in [42]. The algorithm in [42] introduces the lowest position error but with a higher computational time. For the proposed algorithms, the implemented fast array algorithm attains the largest error among the restored parameters. Moreover, the run time of the retrieved peak parameters is of concern. The run time permits the retrieval of larger numbers of peaks. The rate of retrieved peaks is equivalent to the maximum number of recovered peaks divided by the running time. The proposed algorithms achieve a higher robustness. The estimated average peak and position errors of the fourth average combinational algorithm are lower than those of both the slope tangent and fast array algorithms. This algorithm requires a longer

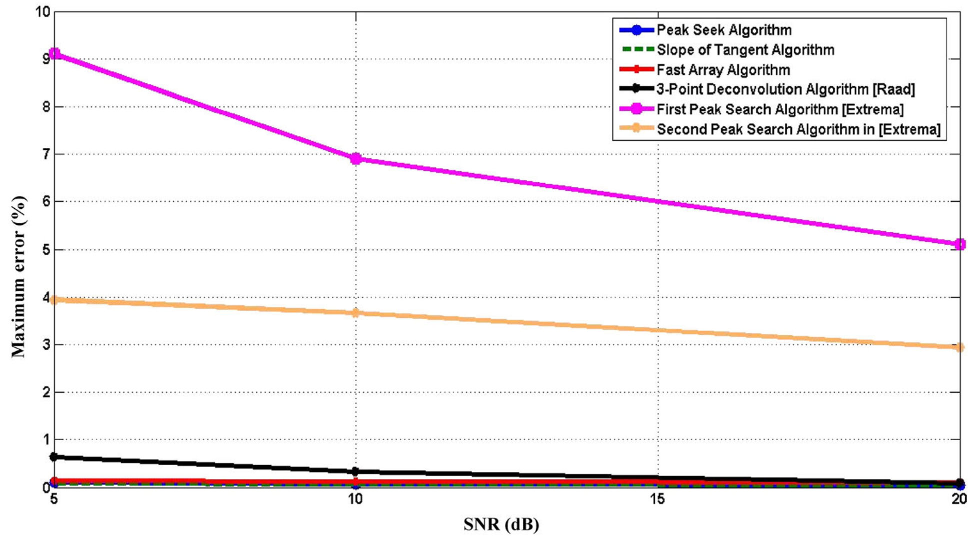

Fig. 24 Maximum peak error between recovered peaks and input pileup against SNR for developed peak recovery algorithms and applied experimental methods in [20, 42]

time compared to the other algorithms because it combines the three algorithms into a single algorithm. The computing time will therefore be increased. The comparison results confirm the robustness of the proposed algorithms. This rate is described as follows:

$$\Re = \frac{\chi}{\beta}, \tag{31}$$

where β and χ denote the central processing (CPU) time and the maximum number of recovered peaks, respectively. The slope of the tangent algorithm consumes the lowest possible time in comparison with other algorithms. The higher computational time is attained by the peak seek algorithm. Hence, the rate of computational peaks owing to the slope tangent algorithm is higher than that of the other algorithms. The accuracy of the underlined algorithms is assessed through a comparison with the experimental results in the literature [20, 42]. The proposed and published algorithms were tested using the same data for a better assessment. The performance of the algorithms under the effects of the WGN is shown in Fig. 24. The highest prediction error of the reconstructed peaks against a variation in the signal-to-noise ratio (SNR) is established in Fig. 24. The 3-point deconvolution algorithm is a widely applied technique in experimental spectrometry systems. The highest peak amplitude error is computed for the 3-point deconvolution algorithm [20]. At SNR = 5 dB, the 3-point deconvolution, peak search with extreme, and second peak search algorithms achieve the highest peak errors of 0.63, 9.1020, and 3.9426, respectively. In addition, the deconvolution filter complexity increases with the number of moving average points. The realized error from the peak search method in [42] is higher than the error of all other algorithms. However, the proposed slope of the tangent algorithm shows a peak amplitude error of 0.093% at SNR = 5 dB. The fast array algorithm shows the highest computational error among the proposed algorithms at all SNR values. This error is due to the higher error attained by the recovered pulse position and the amplitude of this algorithm. This algorithm shows a high sensitivity to noise. Therefore, noise cancelation is essential with the fast array algorithm. The two other proposed algorithms demonstrate a satisfactory accuracy at lower and higher SNR values. The peak seek algorithm shows much better results at a lower SNR. The slope of the tangent algorithm provides a significant accuracy and a lower error at a higher SNR. Hence, noise removal is needed with the proposed fast array algorithm.

In addition, this subsection is concerned with the optimum detection of the peak heights using the ALO algorithm. This optimizer algorithm depends on the selection of a proper retrieval algorithm. Thus, the optimum detection of the peak heights is based on two successive dependent steps. The ALO algorithm is linked individually to the three peak retrieval algorithms. The output of the ALO algorithm depends on the SOP retrieval algorithms. The initial values of the parameters of the ALO algorithm are shown in Table 5. A comparison between the optimum responses of the proposed peak recovery algorithms is

Table 5 Parameter initialization of ALO algorithm

Variable	Value
Number of search agents	10–40
Number of iterations	4–5
Max cycles	500
Upper bound	0–4
Lower bound	10
Max cycle	400–500

Table 6 Optimum parameters of detected peaks of three peak retrieval algorithms using ALO algorithm

Algorithms	Best position	Best cost	Max	Average	Median	Std	Run time (s)
Peak seek algorithm	0.65171 1.0139 1.323 1.5262	0.00095525	1.5262	1.1287	1.1684	0.3814	919.140950
Slope tangent algorithm	6.3855 6.0824 9.1121 7.3742	0.036271	9.1121	7.2385	6.8799	1.3654	1641.490657
Fast array algorithm	8.1472 1.5761 6.5574 7.0605	1.7197	8.1472	5.8353	6.8089	2.9159	1726.889975

introduced in Table 6. This comparison emphasized the best position of the moved ants. In addition, the optimum cost of the nonlinear function taken from the peak retrieval algorithm is evaluated. Several processes are applied on the cost function, such as the average, median, standard deviation, and maximum cost. Four positions are estimated for each peak retrieval algorithm. These positions optimize the operation of each corresponding retrieval algorithm. The lowest cost function of 0.955×10^{-3}, which achieves the optimum value, is attained using the peak seek algorithm. Thus, the corresponding cost parameters (average, median, standard deviation, and maximum cost) of the peak seek algorithm are much lower than those of the other algorithms. However, the variation in the best position by the ALO algorithm for the proposed peak retrieval algorithms of digital alpha spectroscopy is presented in Fig. 25. The best scores are accomplished using the sum of the retrieved peaks by the slope tangent algorithm. In addition, the optimization of the peak seek algorithm shows the lowest scores. From the computational time perspective in Table 6, the proposed peak seeking algorithm shows a better execution time of 919.140950 s. However, the execution time for all algorithms is excessively long. This may be due to the diverse dependent steps of the ALO algorithm. The convergence curves of the ALO algorithm against the number of generations for the proposed peak retrieval algorithms used in digital alpha spectroscopy are illustrated in Fig. 26. The distinction between the proposed algorithms declares the third proposed algorithm with far convergence. However, the convergence of the first proposed peak seek algorithm is much lower than that of all other algorithms. The application of ALO for an optimization of the overlapped alpha peaks requires a much longer execution time. Thus, the use of a superior hardware processor, such as a field programmable gate array, is encouraged. Therefore, the need for a faster algorithm is essential. This is necessary during an interaction at a higher counting rate. Consequently, the optimization process

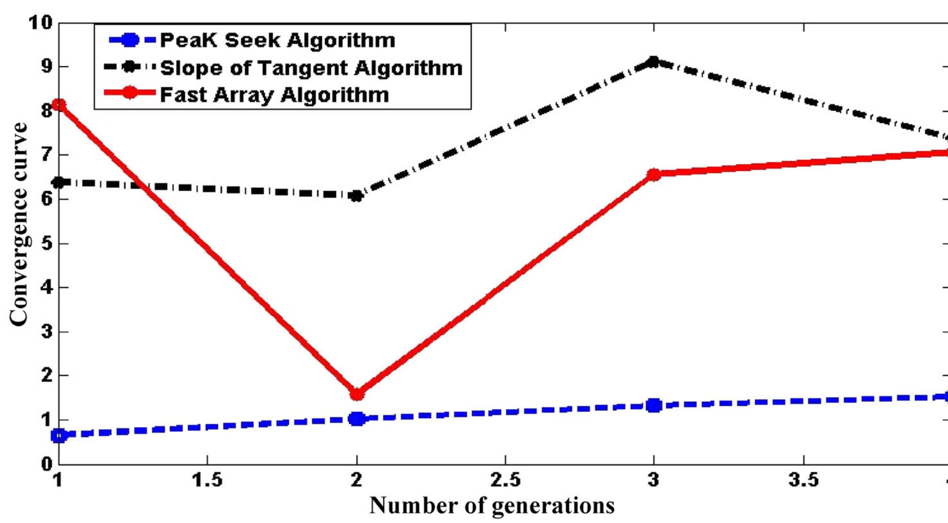

Fig. 25 Variation of best positions by ALO algorithm for proposed peak retrieval algorithms of digital alpha spectroscopy

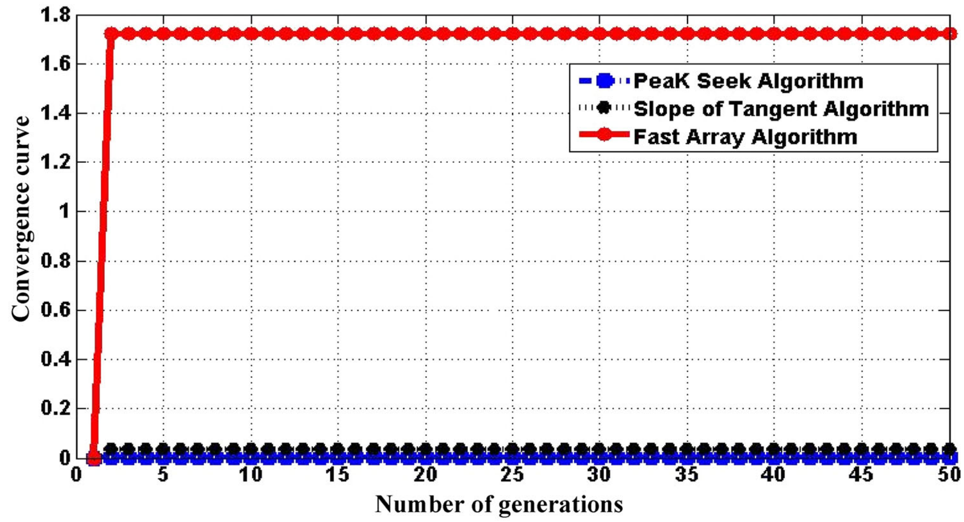

Fig. 26 Convergence curve of ALO algorithm against number of generations for proposed peak retrieval algorithms of digital alpha spectroscopy

described in this paper is continued using the PSO algorithm.

Finally, the optimum detection of SOP alpha peaks is considered using the PSO algorithm, which was adapted to deal with alpha radiation peaks. The initialization parameters of this algorithm are illustrated in Table 7. Table 8 shows the optimum parameters of the detected peaks by the proposed retrieval algorithms using the PSO algorithm. The results of this algorithm are based on a comparison between the proposed peak retrieval algorithms in terms of the provisioning of the optimum cost and position. The best cost of the slope tangent algorithm is the lowest compared to that of the other peak recovery algorithms, but at the expense of the running time. A much longer time is required compared to the other algorithms. The mean, median, and standard deviation of the best cost are determined. The results show much lower values for the peak seek recovery algorithm. The standard deviation, mean, maximum, and minimum values of the best particle positions are estimated. The peak seek algorithm achieves the lowest values compared to the other algorithms.

The changes in the best position and the particle position against the number of swarms of the PSO algorithm for the peak seek algorithm, slope tangent algorithm, and fast array algorithm are shown in Fig. 27a–c, respectively. It should be noted that a significant variation between the particle position and best position was realized by the peak seek algorithm. However, the fast array algorithm introduces an identical change in the best position and the particle position for all swarms. Therefore, it is of primary concern to find the positional error. The errors in the estimated positions against the number of swarms of the PSO algorithm for the proposed peak retrieval algorithms used in digital alpha spectroscopy are shown in Fig. 28. Note that the slope tangent algorithm shows large variations at lower and higher numbers of swarms. However, the fast array algorithm achieves the lowest variation.

Table 7 Parameter initialization of PSO algorithm

Variable	Value
Number of decision variables	10
Max velocity	2
Min velocity	−2
Inertia weight	0.7298
Inertia weight damping ratio	1
Personal learning coefficient	1.4962
Global learning coefficient	1.4962
Bound of variables	[− 10,10]
Maximum number of iterations	10–1000
Swarm size	100
Constriction coefficients, φ_1, φ_2	2.05

The stimulated particle velocity is predicted. Thus, the variation of the best particle velocity against the number of swarms of the PSO algorithm for the proposed peak recovery algorithms used in digital alpha spectroscopy is shown in Fig. 29. It can be observed that the lowest particle velocity is attained by the slope tangent algorithm. This idea is reflected in the higher running time of this algorithm for an estimation of the peak recovery. However, the peak seek algorithm introduces an acceptable velocity for achieving the optimum cost and position. The convergence curve for the PSO algorithm is shown in Fig. 30. This figure demonstrates the change in the convergence curve of the PSO algorithm against the number of generations for the proposed peak recovery algorithms used in digital alpha spectroscopy. The highest value of convergence is obtained by the fast array peak recovery algorithm at all numbers of iterations. However, the lowest value is achieved by the

Table 8 Optimum parameters of peaks detected by proposed retrieval algorithms using PSO algorithm

Algorithms	Cost				Position				Run time (s)
	Best cost	Standard deviation	Median	Average	Standard deviation	Mean	Max	Min	
Peak seek	0.9553×10^{-3}	0	9.5525×10^{-4}	9.5525×10^{-4}	5.4531	0.8383	8.6016	−7.4886	757.394083
Slope tangent	0.036271	9.7634×10^{-17}	0.0363	0.0363	6.3487	2.8220	9.6827	−6.5013	3685.747118
Fast array	1.7197	0	1.7197	1.7197	5.1330	0.7624	8.9619	−8.1831	1623.060307

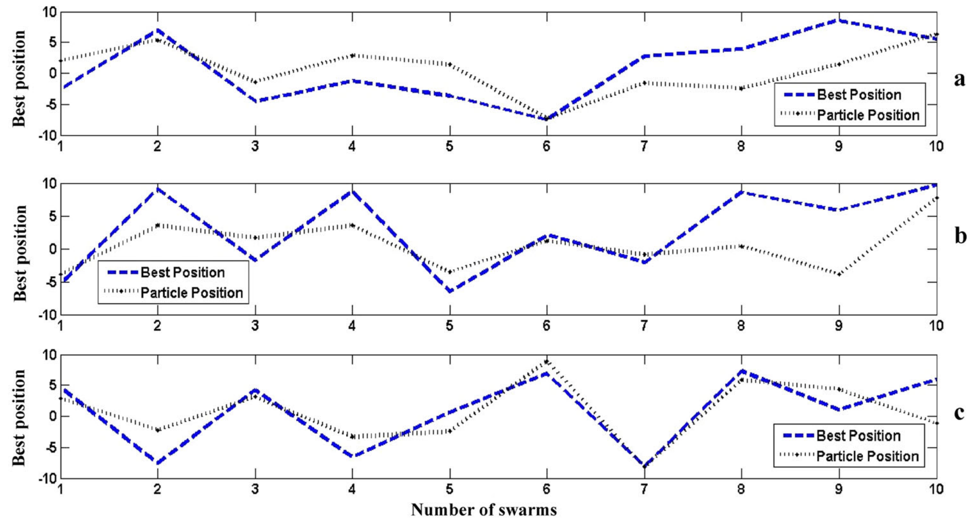

Fig. 27 Variation of best position and particle position against number of swarms of PSO algorithm for **a** peak seek algorithm, **b** slope tangent algorithm, and **c** fast array algorithm

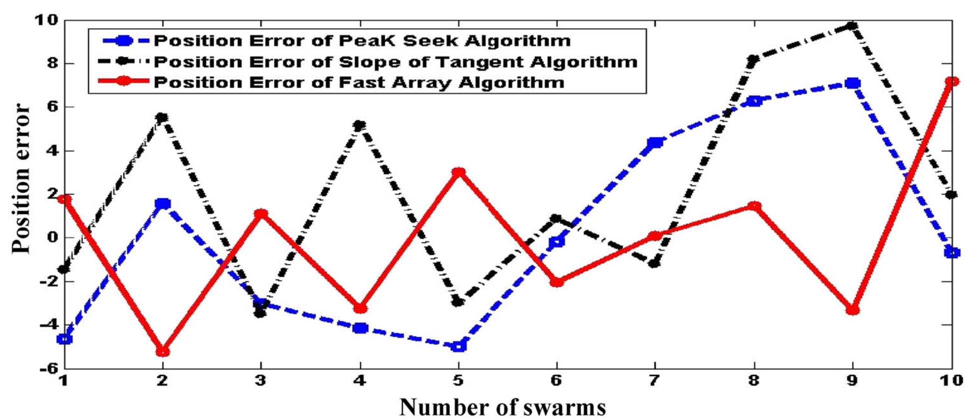

Fig. 28 Error of estimated positions against number of swarms of PSO algorithm for proposed peak retrieval algorithms of digital alpha spectroscopy

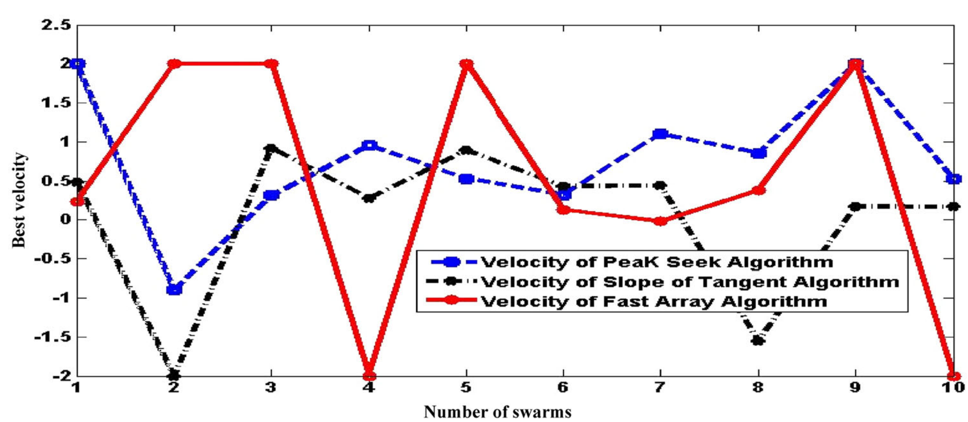

Fig. 29 Variation in best particle velocity against number of swarms of PSO algorithm for proposed peak retrieval algorithms of digital alpha spectroscopy

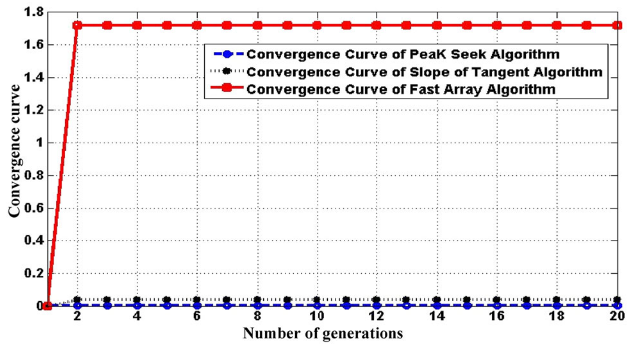

Fig. 30 Convergence curve of PSO algorithm against number of generations for proposed peak retrieval algorithms of digital alpha spectroscopy

proposed peak seek algorithm. The convergence values of the ALO are similar to those of the PSO for optimization of the detected peak of the alpha spectroscopy when using the proposed peak retrieval algorithm. It can be observed that the optimal values of the cost function, particle position, and velocity for the detected peaks by the PSO are much better than those accomplished by the ALO. In addition, the main obstacle of the underlined optimization algorithms is the processing speed. Thus, a fast processing hardware is necessary. In addition, it should be noted that the PSO requires less time than the ALO applying a peak recovery algorithm.

6 Conclusion

The retrieval of SOP peaks caused by high counting rates in digital alpha spectroscopy is the main goal of this study. ALO and PSO optimization algorithms are applied for this purpose. Optimization algorithms were selected for surpassing conventional methods for pulse localization. These algorithms estimate the optimum position of the retrieved pulse. Otherwise, the pulse is illusive and should be rejected. Moreover, each optimization algorithm is linked to the output of one time-domain peak finder algorithm such as the peak seek, slope tangent, and fast array algorithm. The peak finder algorithm feeds its output to one optimization technique. An evaluation of these algorithms is accomplished in a provisioning of the cost function. A comparison between the proposed algorithms with respect to the average error was conducted. The peak seek algorithm introduces preferable results with a special emphasis on the peak height and computational time. In addition, the peak seek algorithm attains the optimum retrieved peak parameters (amplitude and position) through the ALO and PSO algorithms. In addition, it achieves the lowest average error at different SNR values. However, the fast array algorithm provides the worst recovery results of the pulse parameters. Furthermore, the optimum performance of the PSO exceeds that of the ALO algorithm with the time-domain peak finder algorithm for alpha spectroscopy. Validation of the peak retrieval algorithms was conducted through a comparison with previous studies. Optimization algorithms were proved to be superior to traditional techniques for retrieval of SOP alpha peaks at high counting rates.

References

1. A. Alessandrello, C. Broerio, O. Cremonesi et al., A massive thermal detector for alpha and gamma spectroscopy. Nucl. Instrum. Methods Phys. Res. A **440**, 397–402 (2000). https://doi.org/10.1016/S0168-9002(99)00928-6
2. J. Janda, L. Fiserova, Thermal neutron detection using alpha/beta-gamma discrimination circuit. Radiat. Phys. Chem. **156**, 109–114 (2019). https://doi.org/10.1016/j.radphyschem.2018.11.007
3. T.R. Garcia, B. Reinke, W. Windl et al., Alpha spectroscopy for in situ liquid radioisotope measurements. Nucl. Instrum. Methods Phys. Res. A **780**, 119–126 (2015). https://doi.org/10.1016/j.nima.2014.12.062
4. C. Charalambous, M. Aletrari, P. Piera et al., Uranium levels in Cypriot groundwater samples determined by ICP-MS and α-spectroscopy. J. Environ. Radioact. **116**, 187–192 (2013). https://doi.org/10.1016/j.jenvrad.2012.10.008
5. F. Pollastrone, G.C. Cardarilli, M. Riva et al., A clustering algorithm for scintillator signals applied to neutron and gamma patterns identification. Fusion Eng. Des. **146**(Part B), 2110–2114 (2019). https://doi.org/10.1016/j.fusengdes.2019.03.117
6. A.J. Crompton, K.A.A. Gamage, A. Jenkins et al., Alpha particle detection using alpha-induced air radioluminescence: A review and future prospects for preliminary radiological characterization for nuclear facilities decommissioning. Sensors **18**(14), 1015 (2018). https://doi.org/10.3390/s18041015
7. P.S. Lee, C.S. Lee, J.H. Lee, Development of FPGA-based digital signal processing system for radiation spectroscopy. Radiat. Meas. **48**, 12–17 (2013). https://doi.org/10.1016/j.radmeas.2012.11.018
8. A. Stamatopoulos, M. Diakaki, A. Tsinganis et al., An alternative methodology for high counting-loss corrections in neutron time-of-flight measurements. Nucl. Inst. Methods Phys. Res. A **913**, 40–47 (2019). https://doi.org/10.1016/j.nima.2018.10.032
9. X.L. Luo, V. Modamio, J. Nyberg et al., Pulse pile-up identification and reconstruction for liquid scintillator based neutron detectors. Nucl. Instrum. Methods Phys. Res. A **897**, 59–65 (2018). https://doi.org/10.1016/j.nima.2018.03.078
10. A.A. Mowlavi, M.H.H. Yazdi, Monte Carlo simulation of pulse pile-up effect in gamma spectrum of a PGNAA system. Nucl. Instrum. Methods Phys. Res. A **660**(1), 104–107 (2011). https://doi.org/10.1016/j.nima.2011.09.022
11. D.C. Ott, J.L. Tain, A. Gadea et al., Pulse pileup correction of large NaI(Tl) total absorption spectra using the true pulse shape. Nucl. Instrum. Methods Phys. Res. A **430**(2–3), 488–497 (1999). https://doi.org/10.1016/S0168-9002(99)00216-8
12. S. Pomme, How pileup rejection affects the precision of loss-free counting. Nucl. Instrum. Methods Phys. Res. A **432**(2–3), 456–470 (1999). https://doi.org/10.1016/S0168-9002(99)00475-1
13. C. Guerrero, D.C. Ott, E. Mendoza et al., Correction of dead-time and pile-up in a detector array for constant and rapidly varying

counting rates. Nucl. Instrum. Methods Phys. Res. A **777**, 63–69 (2015). https://doi.org/10.1016/j.nima.2014.12.008
14. D.C. Ott, J.L. Tain, A. Gadea et al., Pulse pileup correction of large NaI(Tl) total absorption spectra using the true pulse shape. Nucl. Instrum. Methods Phys. Res. A **430**, 488–497 (1999). https://doi.org/10.1016/S0168-9002(99)00216-8
15. G.F. Knoll, *Radiation Detection and Measurement*, 3rd edn. (Wiley, New Jersey, 2000)
16. S. Usman, A. Patil, Radiation detector deadtime and pile up: a review of the status of science. Nucl. Eng. Technol. **50**(7), 1006–1016 (2018). https://doi.org/10.1016/j.net.2018.06.014
17. R. Grzywacz, Applications of digital pulse processing in nuclear spectroscopy. Nucl. Instrum. Methods Phys Res. B **204**, 649–659 (2003). https://doi.org/10.1016/S0168-583X(02)02146-8
18. Z. Huaiqiang, G. Liangquan, T. Bin et al., Optimal choice of trapezoidal shaping parameters in digital nuclear spectrometer system. Nucl. Sci. Tech. **24**, 060407-1-0604076 (2013)
19. C.T. Angell, Pulse pileup correction in the presence of a large low-energy background. J. Nucl. Sci. Technol. **52**(3), 426–433 (2015). https://doi.org/10.1080/00223131.2014.955067
20. M.W. Raad, M. Deriche, J. Noras et al., A novel approach for pileup detection in gamma-ray spectroscopy using deconvolution. Meas. Sci. Technol. **19**, 065601 (2008). https://doi.org/10.1088/0957-0233/19/6/065601
21. M. Bolic, V. Drndarevic, W. Gueaieb, Pileup correction algorithms for very-high-count-rate gamma-ray spectrometry with NaI(Tl) detectors. IEEE Trans. Instrum. Meas. **59**(1), 122–130 (2010). https://doi.org/10.1109/TIM.2009.2022107
22. E. Barat, T. Dautremer, T. Montagu, J.-C. Trama, A bimodal kalman smoother for nuclear spectrometry. Nucl. Instrum. Methods A **567**, 350–352 (2006). https://doi.org/10.1016/j.nima.2006.05.243
23. R. Coulon, S. Normand, G. Ban et al., Delayed gamma power measurement for sodium-cooled fast reactors. Nucl. Eng. Des. **241**, 339–348 (2011). https://doi.org/10.1016/j.nucengdes.2010.10.002
24. C. Qu, H. Yang, J. Cai et al., DoPS: A double-peaked profiles search method on the RS and SVM. IEEE Access **7**, 106139–106154 (2019). https://doi.org/10.1109/ACCESS.2019.2927251
25. F. Belli, B. Esposito, D. Marocco et al., Jet Efda Contributors, a method for digital processing of pile-up events in organic scintillators. Nucl. Instrum. Methods Phys. Res. A **595**, 512–519 (2008). https://doi.org/10.1016/j.nima.2008.06.045
26. K.M. Langen, P.J. Binns, A.J. Lennox et al., Pileup correction of microdosimetric spectra. Nucl. Instrum. Methods Phys. Res. A **484**(1–3), 595–612 (2002). https://doi.org/10.1016/S0168-9002(01)02014-9
27. S.M. Robinson, S. Stave, A. Lintereur et al., Neutron pileup algorithms for multiplicity counters. Nucl. Instrum. Methods Phys Res. A **748**, 293–297 (2014). https://doi.org/10.1016/j.nima.2014.11.112
28. M. Asai, F.P. Heßberger, A.L. Martens, Nuclear structure of elements with $100 \leq Z \leq 109$ from alpha spectroscopy. Nucl. Phys. A **944**, 308–332 (2015). https://doi.org/10.1016/j.nuclphysa.2015.06.011
29. J. Pechousek, D. Konecny, P. Novak et al., Software emulator of nuclear pulse generation with different pulse shapes and pile-up. Nucl. Instrum. Methods Phys. Res. A **828**, 81–85 (2016). https://doi.org/10.1016/j.nima.2016.05.032
30. X. Zhong, L. Chen, B. Wang et al., A spectrometer with baseline correction and fast pulse pile-up rejection for prompt gamma neutron activation analysis technology. Rev. Sci. Instrum. **89**, 123504-1–123504-8 (2018). https://doi.org/10.1063/1.5049517
31. T. O'Haver, *An Introduction to Signal Processing in Chemical Analysis* (University of Maryland, College Park, 2009), pp. 1–45
32. H. Kılıc, U. Yuzgec, Improved antlion optimization algorithm via tournament selection and its application to parallel machine scheduling. Comput. Ind. Eng. **132**, 166–186 (2019). https://doi.org/10.1016/j.cie.2019.04.029
33. S. Mirjalili, The ant lion optimizer. Adv. Eng. Softw. **83**, 80–98 (2015). https://doi.org/10.1016/j.advengsoft.2015.01.010
34. H. Kılıc, U. Yuzgec, Tournament selection based antlion optimization algorithm for solving quadratic assignment problem. Eng. Sci. Technol. **22**, 673–691 (2019). https://doi.org/10.1016/j.jestch.2018.11.013
35. H. Qi, L.M. Ruan, M. Shi et al., Application of multi-phase particle swarm optimization technique to inverse radiation problem. J. Quant. Spectrosc. Radiat. Transf. **109**(3), 476–493 (2008). https://doi.org/10.1016/j.jqsrt.2007.07.013
36. H. Shahabinejad, N. Vosoughi, Analysis of complex gamma-ray spectra using particle swarm optimization. Nucl. Instrum. Methods Phys Res. A **911**, 123–130 (2018). https://doi.org/10.1016/j.nima.2018.09.156
37. H. Shahabinejad, M. Sohrabpour, A novel neutron energy spectrumunfolding code using particle swarm optimization. Radiat. Phys. Chem. **136**, 9–16 (2017). https://doi.org/10.1016/j.radphyschem.2017.03.033
38. H. Ajdad, Y.F. Baba, A.A. Mers et al., Particle swarm optimization algorithm for optical-geometric optimization of linear fresnel solar concentrators. Renew. Energy **130**, 992–1001 (2018). https://doi.org/10.1016/j.renene.2018.07.001
39. D.-W. Lim, C.-W. Lee, J.-Y. Lim et al., On the particle swarm optimization of cask shielding design for a prototype sodium-cooled fast reactor. Nucl. Eng. Technol. **51**(1), 284–292 (2019). https://doi.org/10.1016/j.net.2018.09.007
40. J. Yang, P. Zhang, L. Zhang et al., Particle swarm optimizer for weighting factor selection in intensity modulated radiation therapy optimization algorithms. Phys. Med. **33**, 136–145 (2017). https://doi.org/10.1016/j.ejmp.2016.12.021
41. S. Ghimire, R.C. Deo, N. Raj et al., Wavelet-based 3-phase hybrid SVR model trained with satellite-derived predictors, particle swarm optimization and maximum overlap discrete wavelet transform for solar radiation prediction. Renew. Sustain. Energy Rev. **113**, 109247 (2019). https://doi.org/10.1016/j.rser.2019.109247
42. K. Lam, W. Zhang, Gamma peak search and peak fitting algorithm for a low-resolution detector with applications in gamma spectroscopy. J. Radioanal. Nucl. Chem. **322**(2), 255–261 (2019). https://doi.org/10.1007/s10967-019-06760-x